

Article

# Power Sharing and Voltage Vector Distribution Model of a Dual Inverter Open-End Winding Motor Drive System for Electric Vehicles

Yi-Fan Jia , Liang Chu, Nan Xu \*, Yu-Kuan Li, Di Zhao  and Xin Tang

State Key Laboratory of Automotive Simulation and Control, Jilin University, Changchun 130022, China; jiajf16@mails.jlu.edu.cn (Y.-F.J.); chuliang@jlu.edu.cn (L.C.); liyk13@mails.jlu.edu.cn (Y.-K.L.); zhaod14@mails.jlu.edu.cn (D.Z.); tangxin16@mails.jlu.edu.cn (X.T.)

\* Correspondence: nanxu@jlu.edu.cn; Tel.: +86-431-8509-5165

Received: 4 January 2018; Accepted: 5 February 2018; Published: 8 February 2018

## Featured Application: control strategy of motor drive system for electric vehicles

**Abstract:** A drive system with an open-end winding permanent magnet synchronous motor (OW-PMSM) fed by a dual inverter and powered by two independent power sources is suitable for electric vehicles. By using an energy conversion device as primary power source and an energy storage element as secondary power source, this configuration can not only lower the DC-bus voltage and extend the driving range, but also handle the power sharing between two power sources without a DC/DC (direct current to direct current) converter. Based on a drive system model with voltage vector distribution, this paper proposes a desired power sharing calculation method and three different voltage vector distribution methods. By their selection strategy the optimal voltage vector distribution method can be selected according to the operating conditions. On the basis of the integral synthesizing of the desired voltage vector, the proposed voltage vector distribution method can reduce the inverter switching frequency while making the primary power source follow its desired output power. Simulation results confirm the validity of the proposed methods, which improve the primary power source's energy efficiency by regulating its output power and lessen inverter switching loss by reducing the switching frequency. This system also provides an approach to the energy management function of electric vehicles.

**Keywords:** electric vehicle; open-end winding; dual inverter; voltage vector distribution; power sharing; energy management

## 1. Introduction

Permanent Magnet Synchronous Motor (PMSM) has been widely used as drive motor on electric vehicles for its high power density, outstanding low-speed torque output and high efficiency [1–5]. However, the back EMF (electromotive force) increases rapidly along with motor speed due to the uncontrollable constant magnetic field of the permanent magnet, which means a higher DC-bus (direct current) voltage and a high-level flux-weakening control are required [6–8]. Furthermore, limited by the restricted energy of power battery with present technology, an extra energy source is often required to reach an acceptable driving range. Usually a DC/DC converter is needed to acquire power distribution and energy management function between the two power sources, which increases system complexity and brings additional losses [9,10].

The above problems can be perfectly solved by using an open-end winding permanent magnet Synchronous Motor (OW-PMSM) fed by two inverters, as shown in Figure 1. Each inverter is powered by an independent power source, and the two power sources are electrically isolated. This

configuration inherently eliminates common-mode currents and can make the two sources virtually cascaded by proper control of dual inverter. Thus, the motor can obtain a higher voltage without increasing DC-bus voltage, resulting in an easier flux-weakening control and a higher top speed [11–14]. By using dual inverter, the actual number of motor phase voltage level is increased. For example, dual two-level inverter operates in three-level mode with equal DC-bus voltages, and operates in four-level mode when the dc voltages are in 2:1 ratio [15]. Moreover, the power flow between the two sources can be transferred through the motor controllably, making the system free of DC/DC converter [15,16].

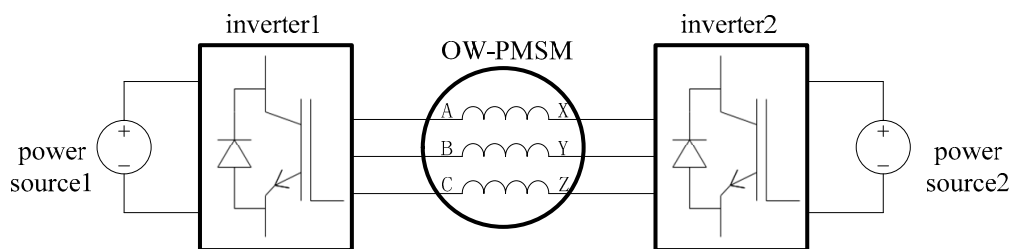


**Figure 1.** Structure of dual inverter open-end winding permanent magnet synchronous motor (OW-PMSM) drive system.

If we define power source1 as primary power source, power source2 as secondary power source, one of the most popular scheme is using a power battery as primary power source, and a floating capacitor as secondary power source. Due to the low internal resistance and high-rate discharge capability, the capacitor often acts as a power buffer, providing the reactive power consumed by the load, and smoothing power output of primary power source by absorbing instantaneous power fluctuation [16–20]. Joon Sung Park et al. proposed a dual inverter strategy for this scheme. By setting inverter2 to take care of reactive voltage and controlling active power flow, the torque and power level of high speed was enhanced, and the voltage of the capacitor was well regulated [20]. A hybrid PWM (pulse-width modulation) based flux-weakening control strategy for this scheme was proposed by Dan Sun et al. A double vector based PWM, utilizing one active vector and one optimal zero vector in a switching period, was applied to inverter1, resulting in the decreasing of switching frequency as well as switching loss. The flux-weakening control strategy also fully utilized the DC-bus voltage and widened motor operating range [21].

However, because of the low energy capacity, using a capacitor as secondary power source usually could not satisfy the requirements of most driving conditions for electric vehicle. Thus, the scheme including some type of energy conversion device, such as an engine generator or fuel cell as primary power source, some type of energy storage element, such as a battery or super capacitor as secondary power source comes into fashion [15,22]. Brian A. Welchko proposed three methods to achieve the combined motor control and energy management functions for this scheme, which are unity power factor control, voltage quadrature control, and optimum inverter utilization control [15]. By choosing the proper method, the energy flow in secondary energy source, the available system voltage to load when secondary energy source is not outputting active power, or the power flow to load can be maximized, respectively. A modulation strategy was proposed by Domenico Casadei et al., able to regulate the power sharing between the power sources by means of a special switching sequence for dual inverter. In addition, the limit of power sharing ratio was determined as a function of the modulation index [23]. However, the proposed strategy could only split the voltage vector linearly so that the modulation ranges of two inverters are underutilized.

In our previous work, we proposed a multi-level current hysteresis modulation algorithm, able to set major power source and switch it at any moment, which could accomplish power distribution between two power sources [24]. However, the proposed methods could only distribute the power between two power sources in a fixed ratio according to the major power source at each working point

of the motor. To control the power flow appropriately, the major power source must be switched many times in a working cycle, just like a PWM controller.

Aiming at electric vehicles with an OW-PMSM driving and powered by two power sources, in this paper, a voltage vector-synthesizing model based on the midpoint voltage, and the power sharing principle are discussed. Then a power sharing calculation method is proposed to acquire the present desired power of primary power source. After that, three voltage vector distribution methods are introduced. The selection strategy of these three methods is then proposed to select the optimal method. On the basis of the integral synthesizing of the desired voltage vector, lowering the inverter switching frequency while making the output power of primary power source follow the desired value with specified accuracy can be achieved. At last a complete simulation of the drive system is executed to verify the control methods proposed.

In particular, the coordination transformations among static three-phase coordinate, static two-phase coordinate and rotary two-phase coordinate in this paper are equivalent power conversions.

## 2. Operating Principle

The control methods proposed by this paper is based on voltage vector generated by dual inverter, so in this section the mathematical system model is built, which provides theoretical support for the voltage vector distribution methods. In addition, the principle of the power sharing and power flow between two power sources are illuminated to support the proposed control methods.

### 2.1. System Modeling

First, we will introduce the concept of mid-point voltage. By equally dividing primary power source and secondary power source into two parts according to their voltages, we can acquire virtual mid-points *m* and *n*. Voltage difference between each inverter leg's output and corresponding mid-point is mid-point phase voltage, and voltage difference between mid-points of the two power sources is mid-point voltage difference. As shown in Figure 2,  $V_{dc1}$  and  $V_{dc2}$  are the DC-bus voltages of primary power source and secondary power source respectively.  $u_{Am}$ ,  $u_{Bm}$  and  $u_{Cm}$  are the mid-point phase voltages of inverter1.  $u_{Xn}$ ,  $u_{Yn}$  and  $u_{Zn}$  are the mid-point phase voltages of inverter2.  $u_{mn}$  is the mid-point voltage difference between the two power sources.

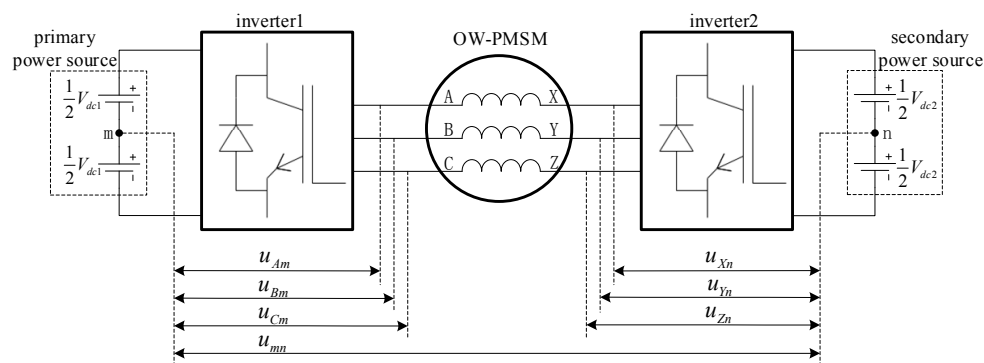


Figure 2. Schematic diagram of mid-point voltage.

The phase voltages of OW-PMSM are affected by both inverters' switching states. Based on Kirchoff's law, the phase voltages of OW-PMSM are determined by Equation (1):

$$\begin{cases} u_{AX} = u_{Am} - u_{Xn} + u_{mn} \\ u_{BY} = u_{Bm} - u_{Yn} + u_{mn} \\ u_{CZ} = u_{Cm} - u_{Zn} + u_{mn} \end{cases} \quad (1)$$

In motor stator plane, the stator voltage vector of OW-PMSM  $\vec{u}_s$  is synthesized by the three phase voltages as follow:

$$\vec{u}_s = \sqrt{\frac{2}{3}}(u_{AX}e^{j0} + u_{BY}e^{j\frac{2\pi}{3}} + u_{CZ}e^{j\frac{4\pi}{3}}) \tag{2}$$

where  $e^{j0}$ ,  $e^{j\frac{2\pi}{3}}$  and  $e^{j\frac{4\pi}{3}}$  are spatial operators, pointing the directions of the three phases' axes respectively.  $\sqrt{\frac{2}{3}}$  is the coefficient of equivalent power conversions. Similarly, the output voltage vector of the two inverters  $\vec{u}_{s1}$  and  $\vec{u}_{s2}$  expressed by mid-point phase voltages are given as:

$$\begin{cases} \vec{u}_{s1} = \sqrt{\frac{2}{3}}(u_{Am}e^{j0} + u_{Bm}e^{j\frac{2\pi}{3}} + u_{Cm}e^{j\frac{4\pi}{3}}) \\ \vec{u}_{s2} = \sqrt{\frac{2}{3}}(u_{Xn}e^{j0} + u_{Yn}e^{j\frac{2\pi}{3}} + u_{Zn}e^{j\frac{4\pi}{3}}) \end{cases} \tag{3}$$

This indicates  $\vec{u}_{s1}$  and  $\vec{u}_{s2}$  are only determined by switching states of the corresponding inverter, and not affected by the other side. Thus,  $\vec{u}_{s1}$  and  $\vec{u}_{s2}$  can be generated by two independent space vector pulse width modulation (SVPWM) controllers.

Substituting Equations (1) and (3) into (2) results in an expression for  $\vec{u}_s$  in terms of  $\vec{u}_{s1}$  and  $\vec{u}_{s2}$ , shown by Equation (4):

$$\vec{u}_s = \vec{u}_{s1} - \vec{u}_{s2} + \sqrt{\frac{2}{3}}u_{mn}(e^{j0} + e^{j\frac{2\pi}{3}} + e^{j\frac{4\pi}{3}}) = \vec{u}_{s1} - \vec{u}_{s2} \tag{4}$$

Because the two power sources are electrically isolated, the mid-point voltage difference  $u_{mn}$  is floating and varying along with the switching states of dual inverter. However, when synthesizing the motor stator voltage vector  $\vec{u}_s$ , the floating  $u_{mn}$  is eliminated as shown in Equation (4). That is because the three phase voltages contain identical component of  $u_{mn}$ , which just counteract each other in motor stator plane. In essence, when the loads of three phase windings are completely symmetrical, the synthesized motor stator voltage vector should be free of zero-sequence component, which means the following equation holds:

$$u_{AX} + u_{BY} + u_{CZ} = 0 \tag{5}$$

By substituting (1) into (5), the value of  $u_{mn}$  can be obtained.

### 2.2. Principle of Power Flow

From Equation (4), we know that  $\vec{u}_s$  can be synthesized by  $\vec{u}_{s1}$  and  $\vec{u}_{s2}$ , where  $\vec{u}_{s1}$  and  $\vec{u}_{s2}$  are generated by two independent SVPWM controllers separately. Thus, when  $\vec{u}_s$  is determined and  $V_{dc1}$ ,  $V_{dc2}$  are measured, the feasible region of voltage vector distribution can be obtained. As shown in Figure 3,  $O_1$  is the origin of vector  $\vec{u}_s$  and  $O_2$  is the end of  $\vec{u}_s$ . Two hexagons indicating the modulation range of the two inverters can be acquired. Hexagon  $A_1B_1C_1D_1E_1F_1$  centering on  $O_1$ , having a side length of  $\sqrt{\frac{2}{3}}V_{dc1}$ , gives the modulation range of inverter1. In the same way, hexagon  $A_2B_2C_2D_2E_2F_2$  centering on  $O_2$  with a side length of  $\sqrt{\frac{2}{3}}V_{dc2}$ , gives the modulation range of inverter2. Vector  $\vec{u}_{s1}$  starts at  $O_1$  and has to end within the range of hexagon  $A_1B_1C_1D_1E_1F_1$ , similarly vector  $\vec{u}_{s2}$  starts at  $O_2$  and has to end within the range of hexagon  $A_2B_2C_2D_2E_2F_2$ . According to Equation (4), the end of  $\vec{u}_{s1}$  and the end of  $\vec{u}_{s2}$  must coincide at one point, assuming it is  $I$ . The overlapping region of the two hexagons  $A_2B_2GD_1E_1H$  corresponds to the feasible region of  $I$ , which also indicates the feasible region of voltage vector distribution.

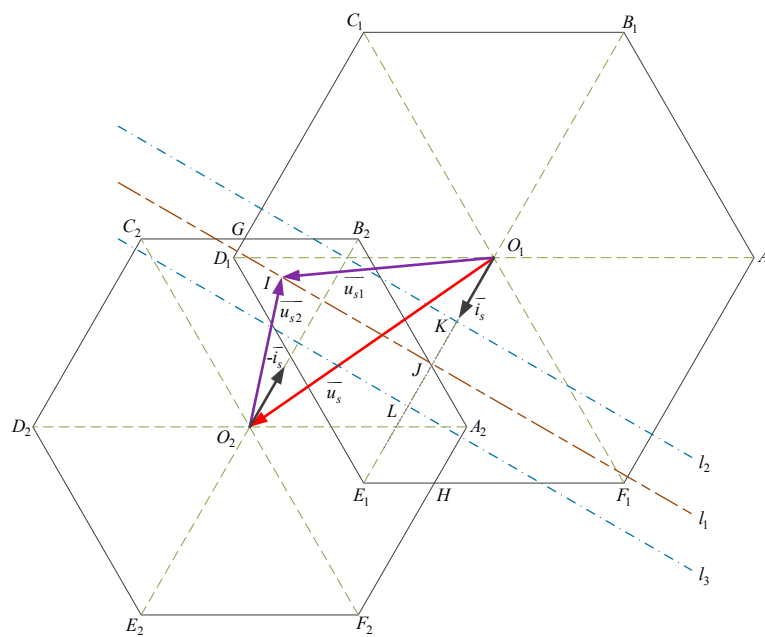


**Figure 3.** Schematic diagram of voltage vector distribution and power sharing.

If the motor stator currents  $i_{AX}$ ,  $i_{BX}$  and  $i_{CX}$  are measured, the stator current vector of OW-PMSM  $\vec{i}_s$  can be obtained as follow:

$$\vec{i}_s = \sqrt{\frac{2}{3}}(i_{AX}e^{j0} + i_{BY}e^{j\frac{2\pi}{3}} + i_{CZ}e^{j\frac{4\pi}{3}}) \tag{6}$$

Then the power sharing of dual inverter can be determined as shown in Equation (7):

$$\begin{cases} P_{inv1} = \vec{u}_{s1} \cdot \vec{i}_s \\ P_{inv2} = \vec{u}_{s2} \cdot \vec{-i}_s = -\vec{u}_{s2} \cdot \vec{i}_s \end{cases} \tag{7}$$

where  $P_{inv1}$  and  $P_{inv2}$  are the output power of inverter1 and inverter2 respectively, positive value means the corresponding inverter is outputting active power and vice versa. It is important to notice the minus sign in the expression of  $P_{inv2}$ . That is because the defined motor phase current polarities are flowing from inverter1 to inverter2, thus the direction of vector  $\vec{i}_s$  on inverter2's point of view is opposite to inverter1's. In Figure 3,  $P_{inv1}$  can be obtained from vector dot product of  $\vec{u}_{s1}$  and  $\vec{i}_s$  at point  $O_1$ , similarly  $P_{inv2}$  can be obtained from vector dot product of  $\vec{u}_{s2}$  and  $\vec{-i}_s$  at point  $O_2$ . Taking inverter1 for example, we have  $P_{inv1} = \vec{u}_{s1} \cdot \vec{i}_s = |\vec{i}_s| |O_1J|$ , where  $|O_1J|$  is the projection of  $\vec{u}_{s1}$  on the direction of  $\vec{i}_s$ . Thus all the available  $\vec{u}_{s1}$  having the same projection  $|O_1J|$  obtain the same value of  $P_{inv1}$ , which is indicated by line  $l_1$  through point  $J$  and orthogonal to  $\vec{i}_s$ . That means all the  $\vec{u}_{s1}$  starting at  $O_1$  and ending on line  $l_1$  gain the same  $P_{inv1}$  at current  $\vec{i}_s$ . Assuming we want the output power of inverter1 limited to the range of  $P_{inv1} \pm \Delta P$ , we can draw two lines parallel to line  $l_1$  and having a distance of  $\frac{\Delta P}{|\vec{i}_s|}$  to  $l_1$  on different side. Those are line  $l_2$  through point  $K$  and line  $l_3$  through point  $L$ , where  $|KJ| = |LJ| = \frac{\Delta P}{|\vec{i}_s|}$ . Thus in prevailing circumstance, the feasible region of point  $I$ , also known as the feasible region of voltage vector distribution, is the intersection set of area  $A_2B_2GD_1E_1H$  and the area between line  $l_2$  and line  $l_3$ .

### 3. Desired Power Sharing Calculation Method

Because an energy conversion device is used as primary power source, we must take its traits for consideration. One is the efficiency characteristic. For example, an engine generator has a best efficiency point and a maximum efficiency curve, operating on which makes the engine under the best economy. The other is the lagging characteristic in response. For example, there is a time lag between opening the throttle and the increasing of engine's output power, or between increasing the hydrogen supply and power uprating of fuel cell. Since the secondary power source is an energy storage device and it does not need additional controls, we set it as a power buffer, to compensate the lacking power or absorb the redundant power outputted by primary power source.

Considering the two traits of the primary power source mentioned above, a desired power sharing calculation method based on a first order inertial element is proposed, as shown in Figure 4.

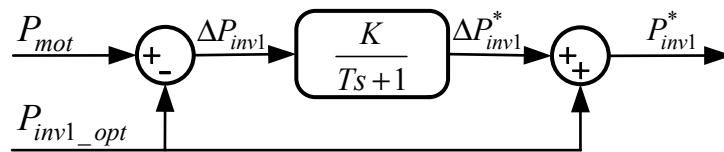


Figure 4. Calculation diagram of desired power of inverter1.

This calculator has two inputs, which are  $P_{mot}$  and  $P_{inv1\_opt}$ . Where  $P_{mot}$  is the input power of OW-PMSM, identical to the summation of two inverters' output power, and can be determined as follow:

$$P_{mot} = \vec{u}_s \cdot \vec{i}_s \tag{8}$$

$P_{inv1\_opt}$  is the optimal output power of inverter1, under which the primary power source obtains maximum efficiency.  $P_{inv1\_opt}$  can be set as a constant, corresponding to the best efficiency point; or set as a variable, corresponding to the maximum efficiency curve, following the changes of its output power. Then the power deviation of inverter1  $\Delta P_{inv1}$  can be obtained by subtracting  $P_{inv1\_opt}$  from  $P_{mot}$ :

$$\Delta P_{inv1} = P_{mot} - P_{inv1\_opt} \tag{9}$$

$\Delta P_{inv1}$  indicates the difference between the total desired power and the ideal power output of inverter1. Thus, we use  $\Delta P_{inv1}$  as the input of the first order inertial element, to generate the compensating power of inverter1. In the frequency domain, we have:

$$\Delta P_{inv1}^*(s) = \frac{K}{Ts + 1} \Delta P_{inv1}(s) \tag{10}$$

where  $\Delta P_{inv1}^*$  is the compensating power of inverter1,  $K$  and  $T$  are the gain and the time constant of the inertial element, respectively. In the time domain,  $\Delta P_{inv1}^*$  and  $\Delta P_{inv1}$  satisfy the following differential equation:

$$T \frac{d}{dt} \Delta P_{inv1}^*(t) + \Delta P_{inv1}^*(t) = K \Delta P_{inv1}(t) \tag{11}$$

In a discrete system, the current  $\Delta P_{inv1}^*$  can be obtained by Equation (12), where  $\Delta P_{inv1}^*(t)$  is the value of  $\Delta P_{inv1}^*$  in current sample step and  $\Delta T$  is the step size of the system.

$$\Delta P_{inv1}^*(t) = \frac{K \Delta P_{inv1}(t) - \Delta P_{inv1}^*(t - \Delta T)}{T} \Delta T + \Delta P_{inv1}^*(t - \Delta T) \tag{12}$$

After  $\Delta P_{inv1}^*$  is obtained, the desired output power of inverter1  $P_{inv1}^*$  can be determined:

$$P_{inv1}^* = P_{inv1\_opt} + \Delta P_{inv1}^* \tag{13}$$

By adjusting  $K$  and  $T$ , different power sharing characteristics can be achieved. We have  $K \in [0, 1]$ , and it affects the response amplitude of  $\Delta P_{inv1}^*$ . The larger  $K$  is, the greater amplitude  $\Delta P_{inv1}^*$  responds to  $\Delta P_{inv1}$ . For example, when  $K = 0$ , we have  $P_{inv1}^* = P_{inv1\_opt}$  at all time, totally regardless of the influence of  $\Delta P_{inv1}$ . In this circumstance, the efficiency of the primary power source is maximized, but the secondary power source will also take the largest power fluctuation. When  $K = 1$ ,  $P_{inv1}^*$  is completely following  $P_{mot}$  except the lag caused by the inertial element. In this circumstance, the power fluctuation of the primary power source will rise, the operating time in high efficiency area and the average efficiency will drop, but the secondary power source is not expected to supply any active power regardless of the influence of the inertial element. The time constant  $T$  affects speed and sensitivity of  $\Delta P_{inv1}^*$  responding to  $\Delta P_{inv1}$ . The larger  $T$  is, the more lag and inertia is in response.

#### 4. Voltage Vector Distribution Method

This section deals with three different voltage vector distribution methods and their selection strategy. Because all these voltage vector distribution methods need to judge whether the inverter desired voltage vector is in the modulation range of the corresponding inverter, the judgmental algorithm will be introduced first.

##### 4.1. Voltage Vector Over Range Judgmental Algorithm

The voltage vector over range judgmental algorithm is derived from the SVPWM strategy. It is used to calculate the proportions of adjacent basic vector for synthesizing desired voltage vector of a single inverter [25]. The calculation result can also indicate whether the desired voltage vector is in the modulation range, which is what we need here.

The desired voltage vector is given in static two-phase coordinate, which are D-axis component  $u_D^*$  and Q-axis component  $u_Q^*$ . As shown in Figure 5a, axis  $J$ ,  $K$  and  $L$  are distributed in circular uniform. The projection of the desired voltage vector on axis  $J$ ,  $K$  and  $L$ , defined as  $j$ ,  $k$  and  $l$  respectively, can be obtained by Equation (14):

$$\begin{cases} j = \frac{u_Q^*}{2} \\ k = \frac{\sqrt{3}u_D^*}{2} - \frac{u_Q^*}{2} \\ l = -\frac{\sqrt{3}u_D^*}{2} - \frac{u_Q^*}{2} \end{cases} \quad (14)$$

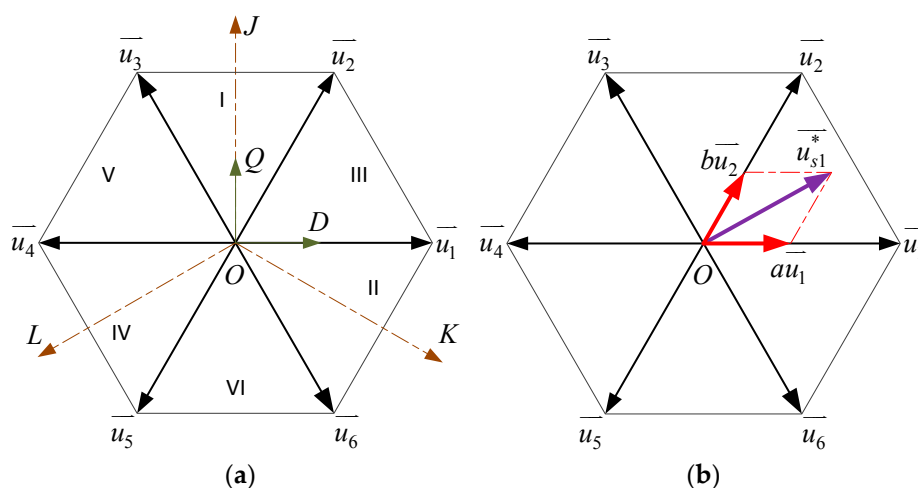


**Figure 5.** Sector partition and voltage vector synthesizing of space vector pulse width modulation (SVPWM). (a) Sector partition; (b) voltage vector synthesis.

Then the sector number  $N$  can be determined as follow:

$$N = \text{sign}(j) + 2\text{sign}(k) + 4\text{sign}(l) \tag{15}$$

where  $\text{sign}$  is the sign function, we have  $\text{sign}(x) = 1$  if  $x > 0$ , otherwise we have  $\text{sign}(x) = 0$ . There are six sectors in total, and the sector number is represented by roman numerals shown in Figure 5a. The proportion parameters  $x, y$  and  $z$  can be calculated using  $u_D^*$  and  $u_Q^*$  by Equation (16), where  $V_{dc}$  is the DC-bus voltage of the corresponding inverter.

$$\begin{cases} x = \frac{\sqrt{2}u_Q^*}{V_{dc}} \\ y = \frac{2u_D^* + \sqrt{3}u_Q^*}{\sqrt{6}V_{dc}} \\ z = \frac{-2u_D^* + \sqrt{3}u_Q^*}{\sqrt{6}V_{dc}} \end{cases} \tag{16}$$

Afterwards, the proportions of adjacent basic vectors to synthesize desired voltage vector, defined as  $a$  and  $b$ , can be obtained by distributing the three proportion parameters according to the sector number, which is shown in Table 1.

**Table 1.** Relation table for a, b and N.

N	0	1	2	3	4	5	6
a	0	z	y	-z	-x	x	-y
b	0	y	-x	x	z	-y	-z

As shown in Figure 5b, taking inverter1 as an example, the desired voltage vector  $\vec{u}_{s1}^*$  lies in Sector III, and is synthesized by the adjacent basic vectors  $\vec{u}_1$  and  $\vec{u}_2$ . We have:

$$\vec{u}_{s1}^* = a\vec{u}_1 + b\vec{u}_2 \tag{17}$$

$a + b \leq 1$  indicates the desired voltage vector is within the range of the hexagon and can be modulated. Otherwise when  $a + b > 1$ , it means the desired voltage vector is out of the modulation range and cannot be generated integrally.

#### 4.2. Low Switching Frequency Method

In a SVPWM control period, there are two switch commutations of each inverter leg normally. Thus, there are six switch commutations of all three legs in a single inverter. When using the dual inverter configuration, the number of switch commutations is doubled. This can cause considerable inverter switching loss and lower the inverter efficiency. However, if one inverter is forced to output only basic voltage vectors or zero vector, there is no switch commutation during the modulation period because the desired voltage vector does not need to be synthesized by two adjacent basic vectors. Thus, the switching frequency of this clamped inverter can be lower to zero if the switch commutations at the junction of modulation periods are ignored. By clamping inverter1 to output only basic voltage vectors and zero vector, the low switching frequency method can reduce the total inverter switching frequency by nearly a half, thus the inverter switching loss is significantly reduced. The desired voltage vector of inverter1  $\vec{u}_{s1}^*$  will be chosen among zero vector and basic voltage vectors lying in the feasible region of voltage vector distribution mentioned in Section 2.2, the one makes inverter1's output power closest to the desired value  $P_{inv1}^*$  will be selected.

The specific algorithm will be introduced as follow. First, matrix  $M_{us1}$  with a size of  $4 \times 7$  is introduced. Each row of  $M_{us1}$  represents a candidate of voltage vectors, including six basic voltage vectors and one zero vector. The first two lines of  $M_{us1}$  are assigned as follow:

$$\begin{cases} M_{us1}(1,:) = \sqrt{\frac{2}{3}}U_{dc1} \circ [0, 1, \frac{1}{2}, -\frac{1}{2}, -1, -\frac{1}{2}, \frac{1}{2}] \\ M_{us1}(2,:) = \sqrt{\frac{2}{3}}U_{dc1} \circ [0, 0, \frac{\sqrt{3}}{2}, \frac{\sqrt{3}}{2}, 0, -\frac{\sqrt{3}}{2}, -\frac{\sqrt{3}}{2}] \end{cases} \tag{18}$$

where  $M_{us1}(n, :)$  means the nth line of matrix  $M_{us1}$ , and “ $\circ$ ” is the operator of Hadamard product, meaning the multiplication of each corresponding element of the two participant matrixes.  $M_{us1}(1, :)$  indicates the D-axis components of each candidate vector, while  $M_{us1}(2, :)$  indicates the Q-axis components. Then the third line of  $M_{us1}$  can be calculated, which indicates inverter1’s output power of the corresponding candidate vector:

$$M_{us1}(3,:) = M_{us1}([1,2],:)^T \times [i_D, i_Q]^T \tag{19}$$

where  $i_D$  and  $i_Q$  are D-axis component and Q-axis component of  $\vec{i}_s$  respectively. The difference between inverter1’s output power of each candidate vector and the desired value  $P_{inv1}^*$  can be obtained by Equation (20), assigned to the fourth line of  $M_{us1}$ :

$$M_{us1}(4,:) = |M_{us1}(3,:) - P_{dc1}^*| \tag{20}$$

Then these power difference values of inverter1 are sorted in ascending sequence. Afterwards the corresponding candidate vectors are checked respectively in the sorted sequence to verify whether it is in the feasible region until we get a positive result.

The specific procedure is introduced as follow. First, obtain inverter2’s voltage vector of the corresponding candidate vector of inverter1 by  $\vec{u}_{s2}^* = \vec{u}_{s1}^* - \vec{u}_s^*$ , which is modified from Equation (4). Then whether this voltage vector is within the modulation range of inverter2 or not is checked by voltage vector over range judgmental algorithm introduced in sector 4.1. If the result is positive, the current candidate vector of inverter1 is valid. Otherwise the next candidate vector in the sorted sequence will be checked until the voltage vector distribution is confirmed valid.

Then the present candidate vector is assigned to inverter1’s desired voltage vector, denoted by  $\vec{u}_{s1\_LF}^*$ , where the subscript LF means Low Frequency. The difference between inverter1’s output power corresponding to  $\vec{u}_{s1\_LF}^*$  and the desired value  $P_{inv1}^*$  can be obtained from the corresponding element in  $M_{us1}(4, :)$ , recorded as  $D_{P_{inv1\_LF}}$ , which is necessary in the selection strategy of voltage vector distribution methods.  $D_{P_{inv1\_LF}}$  indicates inverter1’s power following deviation of the low switching frequency method. If all the candidate vectors are verified beyond the feasible region, the flag of low switching frequency method  $F_{LF}$  will be set to 0, meaning the low switching frequency method is unavailable in current situation; otherwise  $F_{LF}$  will be set to 1, indicating the low switching frequency method is valid.

There are two examples shown in Figure 6. The meanings of lines, points, and vectors are the same with Figure 3. The numbers next to vertexes of the hexagon centered on  $O_1$  indicate the rankings of the corresponding candidate vectors in the sorted sequence, respectively. In the first situation, the first candidate vector in the sequence, whose endpoint is closest to line  $l_1$ , is within the feasible region, so it is chosen to be  $\vec{u}_{s1\_LF}^*$ . However, in the second situation, the first two candidate vectors indicated by dashed lines are both invalid, thus the third candidate vector in the sequence is chosen to be  $\vec{u}_{s1\_LF}^*$ , making inverter1’s power following deviation bigger than the first situation.

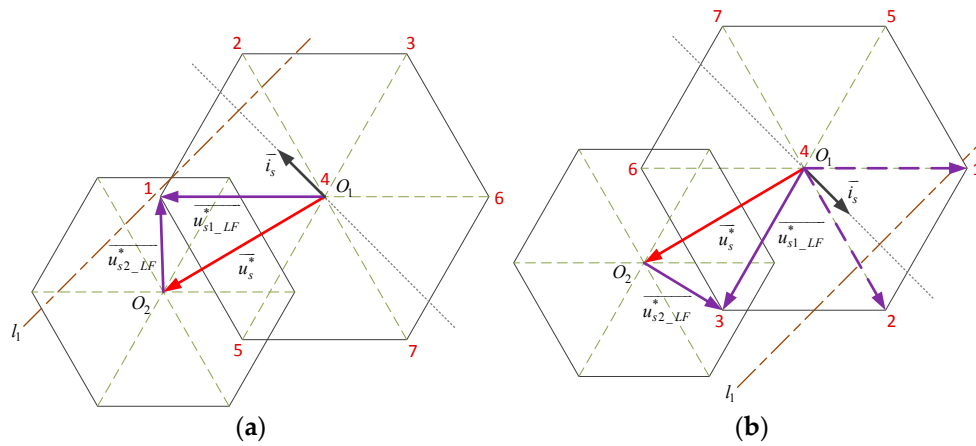


**Figure 6.** Voltage vector distribution examples of low switching frequency method. (a) First situation; (b) second situation.

### 4.3. Accurate Power Following Method

Because low switching frequency method only uses basic voltage vectors and zero vector, the difference of inverter1’s output power between actual and desired value, known as inverter1’s power following deviation, is not minimized. The accurate power following method is proposed to solve this problem when this deviation of low switching frequency method is beyond the tolerance range. The principle of this method is simple: to generate inverter1’s desired voltage vector in phase with  $\vec{i}_s$ , and its amplitude is determined by the desired output power of inverter1, making inverter1’s power following deviation fully eliminated. The collinearity of  $\vec{u}_{s1}$  and  $\vec{i}_s$  could also make inverter1 free of bearing any reactive power.

The specific algorithm will be introduced as follow. First, the amplitude of  $\vec{i}_s$  is obtained using its D-axis and Q-axis components by Equation (21):

$$|\vec{i}_s| = \sqrt{i_D^2 + i_Q^2} \tag{21}$$

Then the amplitude of inverter1’s desired voltage vector can be determined as follow, which makes the corresponding output power of inverter1 equal to the desired value  $P_{inv1}^*$ .

$$|\vec{u}_{s1}^*| = \frac{P_{inv1}^*}{|\vec{i}_s|} \tag{22}$$

Therefore,  $\vec{u}_{s1}^*$  can be obtained by Equation (23) to be in phase with  $\vec{i}_s$ :

$$\vec{u}_{s1}^* = \frac{\vec{i}_s}{|\vec{i}_s|} |\vec{u}_{s1}^*| \tag{23}$$

Afterwards the voltage vector over range judgmental algorithm is executed to check whether the current calculated  $\vec{u}_{s1}^*$  is within the modulation range of inverter1. If the result is positive, the current calculated  $\vec{u}_{s1}^*$  will be assigned to inverter1’s desired voltage vector  $\vec{u}_{s1\_AF}^*$ , where the subscript AF means Accurate Following. Otherwise, the current calculated  $\vec{u}_{s1}^*$  need to be shortened to the boundary of inverter1’s modulation range by the following procedure.

We define the proportions of adjacent basic vectors for synthesizing the current calculated  $\vec{u}_{s1}^*$  as  $a'_1$  and  $b'_1$ , which are the results from the voltage vector over range judgmental algorithm, and we

have  $a'_1 + b'_1 > 1$  so the current calculated  $\vec{u}_{s1}^*$  is beyond the modulation range. To make  $a_1 + b_1 = 1$ , we have:

$$\begin{cases} a_1 = \frac{a'_1}{a'_1 + b'_1} \\ b_1 = \frac{b'_1}{a'_1 + b'_1} \end{cases} \quad (24)$$

where  $a_1$  and  $b_1$  are the proportions of adjacent basic vectors for the shortened  $\vec{u}_{s1}^*$ , which is on the boundary of inverter1's modulation range. Then the amplitude of this shortened  $\vec{u}_{s1}^*$  can be obtained by Equation (25):

$$|\vec{u}_{s1}^*| = \sqrt{\frac{2}{3}} U_{dc1} \sqrt{1 - a_1 b_1} \quad (25)$$

Afterwards, the shortened  $\vec{u}_{s1}^*$  can be obtained by using Equation (23) again. Then the shortened  $\vec{u}_{s1}^*$  can be assigned to  $\vec{u}_{s1\_AF}^*$ . In addition, the difference between inverter1's output power corresponding to  $\vec{u}_{s1\_AF}^*$  and the desired value  $P_{inv1}^*$ , denoted by  $D_{P_{inv1\_AF}}$ , needs to be calculated by Equation (26), which is necessary in the selection strategy of voltage vector distribution methods.

$$D_{P_{inv1\_AF}} = |\vec{u}_{s1\_AF}^* \cdot \vec{i}_s - P_{inv1}^*| \quad (26)$$

Finally, obtain  $\vec{u}_{s2}^*$  by  $\vec{u}_{s2}^* = \vec{u}_{s1}^* - \vec{u}_s^*$  from Equation (4). Then check whether it is within the modulation range of inverter2. If not, the flag of accurate power following method  $F_{AF}$  will be set to 0, meaning the accurate power following method is unavailable in current situation; otherwise  $F_{AF}$  will be set to 1, indicating the calculated  $\vec{u}_{s1\_AF}^*$  is valid.

There are two examples shown in Figure 7. In the first situation, line  $l_1$  intersects  $\vec{i}_s$ 's extension line inside inverter1's modulation range, so inverter1's power following deviation  $D_{P_{inv1\_AF}}$  is completely eliminated. However, in the second situation, the intersection point of line  $l_1$  and  $\vec{i}_s$ 's extension line is beyond inverter1's modulation range. Thus,  $\vec{u}_{s1}^*$  must be shortened to the boundary of this hexagon. Unfortunately, after being shortened,  $\vec{u}_{s1}^*$  is also not in the feasible range of voltage vector distribution because the corresponding  $\vec{u}_{s2}^*$  is out of inverter2's modulation range. Thus, in this situation, the accurate power following method is unavailable.

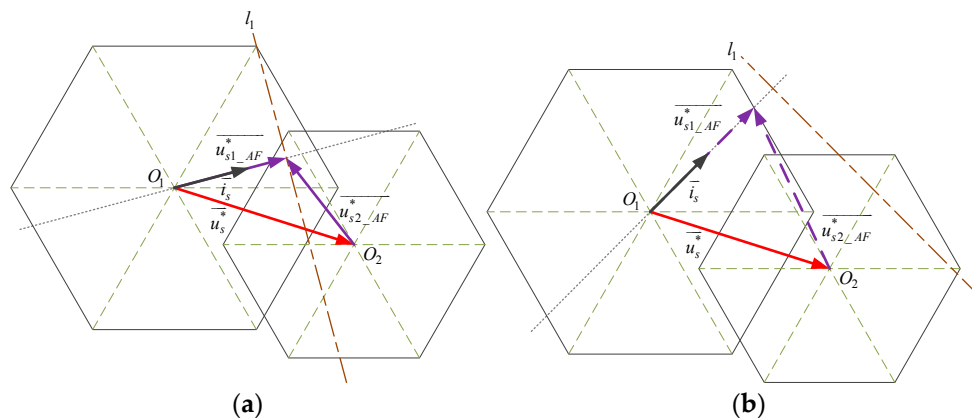


**Figure 7.** Voltage vector distribution examples of accurate power following method; (a) first situation; (b) second situation.

#### 4.4. Linear Partition Method

From Equation (4) we know, when the output voltage vectors of two inverters are 180° out of phase, meaning  $\vec{u}_{s1}$  and  $\vec{u}_{s2}$  are collinear but in the opposite direction, the synthesized  $\vec{u}_s$  has the maximum amplitude. Thus, if we assign  $\vec{u}_{s1}^*$  and  $\vec{u}_{s2}^*$  by linearly partition  $\vec{u}_s$  in the proper position, the possibility of  $\vec{u}_{s1}^*$  and  $\vec{u}_{s2}^*$  in the feasible region can be maximized. This is the strategy of the linear partition method. If both the two methods above have failed to distribute the voltage vectors efficiently, the linear partition method is the last chance. Even if it fails to generate the desired stator voltage vector  $\vec{u}_s^*$  integrally with the limitation of two inverters' DC-bus voltages, in which situation the two hexagons centered on  $O_1$  and  $O_2$  have no overlapping region, the linear partition method can provide a  $\vec{u}_s$  having the same direction and the nearest amplitude with  $\vec{u}_s^*$ .

The specific algorithm will be introduced as follow. First, the amplitude of  $\vec{u}_s^*$  is calculated using its D-axis and Q-axis components as follow:

$$|\vec{u}_s^*| = \sqrt{u_D^{*2} + u_Q^{*2}} \tag{27}$$

Then the desired amplitude of  $\vec{u}_{s1}^*$  can be obtained by Equation (28), making the corresponding output power of inverter1 follows  $P_{inv1}^*$  accurately.

$$|\vec{u}_{s1}^*| = \frac{P_{inv1}^*}{\vec{u}_s^* \cdot \vec{i}_s} |\vec{u}_s^*| \tag{28}$$

Similar to Equation (23),  $\vec{u}_{s1}^*$  can be obtained as follow to be in phase with  $\vec{u}_s^*$ :

$$\vec{u}_{s1}^* = \frac{\vec{u}_s^*}{|\vec{u}_s^*|} |\vec{u}_{s1}^*| \tag{29}$$

Then the voltage vector over range judgmental algorithm is executed to check whether the current calculated  $\vec{u}_{s1}^*$  is within the modulation range of inverter1. If the answer is negative, the current calculated  $\vec{u}_{s1}^*$  need to be shortened to the boundary of inverter1's modulation range by the procedure introduced in sector 4.3, that is using Equations (24), (25) and (29) in turn.

Afterwards, obtain  $\vec{u}_{s2}^*$  by  $\vec{u}_{s2}^* = \vec{u}_{s1}^* - \vec{u}_s^*$ , which is modified from Equation (4). Then check whether  $\vec{u}_{s2}^*$  is within the modulation range of inverter2. If positive, the latest calculated  $\vec{u}_{s1}^*$  will be assigned to inverter1's desired voltage vector  $\vec{u}_{s1\_LP}^*$ , where the subscript LP means Linear Partition. Otherwise, the current calculated  $\vec{u}_{s2}^*$  need to be shortened to the boundary of inverter2's modulation range by the same way with  $\vec{u}_{s1}^*$ . After  $\vec{u}_{s2}^*$  is shortened, we need to recalculate the corresponding  $\vec{u}_{s1}^*$  by  $\vec{u}_{s1}^* = \vec{u}_s^* + \vec{u}_{s2}^*$ , and check whether it is within the modulation range again. If not, shorten it to the boundary of its modulation range. Finally the recalculated  $\vec{u}_{s1}^*$  can be assigned to  $\vec{u}_{s1\_LP}^*$ . Similarly, the difference between inverter1's output power corresponding to  $\vec{u}_{s1\_LP}^*$  and the desired value  $P_{inv1}^*$ , denoted by  $D_{P_{inv1\_LP}}$ , needs to be calculated for voltage vector distribution method selection strategy. Equation (26) is also suitable for this occasion.

There are four examples shown in Figure 8. In the first situation, line  $l_1$  intersects  $\vec{u}_s^*$  right inside the feasible range of voltage vector distribution, thus the first calculated  $\vec{u}_{s1}^*$  is valid. Under this circumstance the output power of inverter1 follows  $P_{inv1}^*$  accurately. In the second situation,  $P_{inv1}^*$  is too big so line  $l_1$  is completely out of inverter1's modulation range. Thus,  $\vec{u}_{s1}^*$  has to be shortened to the

boundary of the hexagon centered on  $O_1$ . In the third situation, the first calculated  $\vec{u}_{s1}^*$ , which makes the output power of inverter1 equals to  $P_{inv1}^*$ , is out of feasible range of voltage vector distribution because the corresponding  $\vec{u}_{s2}^*$  is beyond its modulation range. Thus, after  $\vec{u}_{s2}^*$  is shortened to the hexagon centered on  $O_2$ ,  $\vec{u}_{s1}^*$  is recalculated to compensate the shortage. In the fourth situation, the amplitude of  $\vec{u}_s^*$  is too big so that the two hexagons centered on  $O_1$  and  $O_2$  have no overlapping region. Thus,  $\vec{u}_{s1}^*$  and  $\vec{u}_{s2}^*$  both reached their maximum amplitude collinearly with  $\vec{u}_s^*$  in the opposite direction to synthesize  $\vec{u}_s$ , which is the best available result.

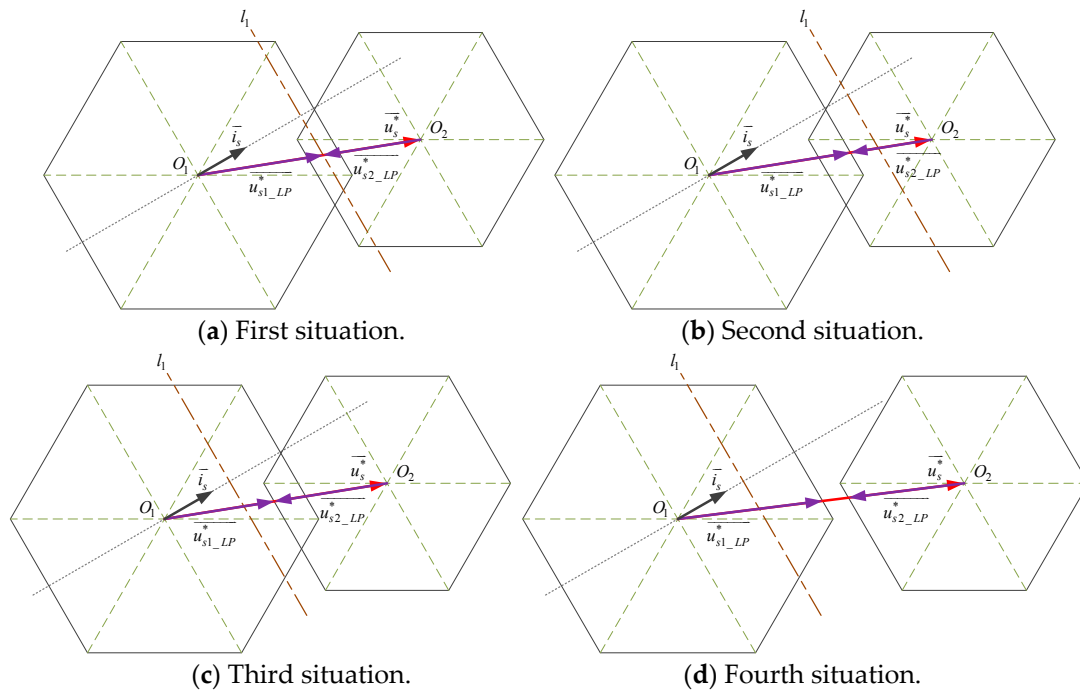


Figure 8. Voltage vector distribution examples of linear partition method.

#### 4.5. Voltage Vector Distribution Method Selection Strategy

Each of these three voltage vector distribution methods introduced above has worked out a result to distribute voltage vectors generated by dual inverter to synthesize the desired stator voltage vector of OW-PMSM. The voltage vector distribution method selection strategy deals with the results from these voltage vector distribution methods by selecting the optimal one as the final result of voltage vector distribution.

The general idea of this selection strategy is expounded as follow. We have three evaluation indexes, which are the accurate synthesizing of desired stator voltage vector, the following of inverter1's desired output power in acceptable accuracy, and the reduction of inverter switching frequency, ranked from highest priority to lowest. In other words, by priority, first we need to ensure the voltage vector distribution result can generate the desired stator voltage vector or as integrally as possible. Based on that, we try to make inverter1's output power follow the desired value in a specific tolerance range. After these two conditions are met, we can think about lowering the inverter switching frequency. The best situation is these three conditions are all satisfied. Otherwise, we discard the reduction of inverter switching frequency. Then we give up the accurate power following of inverter1. At least the synthesizing of desired voltage vector has to be ensured.

For the second condition mentioned above, we need to define the inverter1's maximum power following deviation, denoted by  $D_{P_{inv1\_max}}$ . If inverter1's output power is within the range of  $[P_{inv1}^* - D_{P_{inv1\_max}}, P_{inv1}^* + D_{P_{inv1\_max}}]$ , we consider inverter1's output power is following the desired

value within tolerance range.  $D_{P_{inv1\_max}}$  can be adjusted according to the control requirements of the primary power source.

The specific algorithm of this selection strategy will be introduced as follow. First, the flag of low switching frequency method  $F_{LF}$  is checked. If  $F_{LF} = 1$ , meaning the low switching frequency method is available, the selection will be made between the low switching frequency method and the accurate power following method. Then three conditions are checked, which are  $F_{AF} = 0$ ,  $D_{P_{inv1\_LF}} \leq D_{P_{inv1\_AF}}$ , and  $D_{P_{inv1\_LF}} \leq D_{P_{inv1\_max}}$ . If anyone of these conditions is met, indicating the low switching frequency method meets inverter1’s accurate power following condition or has a better performance in inverter1’s power following, the low switching frequency method will be selected. If all these three conditions are not met, the accurate power following method will be selected. However, if  $F_{LF} = 0$ , meaning the low switching frequency method is invalid in current situation, the selection will have to be made between the accurate power following method and the linear partition method. When  $F_{AF} = 1$  and  $D_{P_{inv1\_AF}} \leq D_{P_{inv1\_LP}}$  are both met, indicating the accurate power following method is available and performs better in inverter1’s power following, the accurate power following method will be selected. Otherwise, the linear partition method will be selected to synthesize the desired stator voltage vector as integrally as possible. The flowchart of the voltage vector distribution method selection strategy is shown in Figure 9.

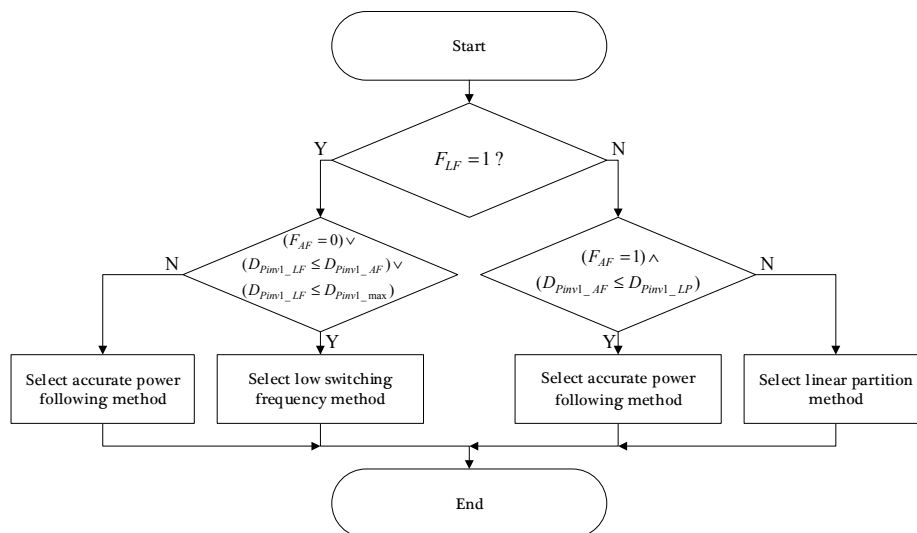


Figure 9. Flowchart of the voltage vector distribution method selection strategy.

### 5. Drive System Simulation

In this sector the overall configuration of the proposed system is summarized and the simulation results of the proposed methods are analyzed.

#### 5.1. Overall Configuration

The overall configuration of the proposed system is shown in Figure 10. It consists of two parts, which are the drive system circuit and the drive system controller. The drive system circuit has the same structure as the system shown in Figure 1, equipped with current sensors measuring the phase currents of OW-PMSM, and voltage sensors measuring DC-bus voltages of dual inverter. The capacitors C1 and C2 are used to filter the voltage fluctuation of the power sources and provide reactive power needed.

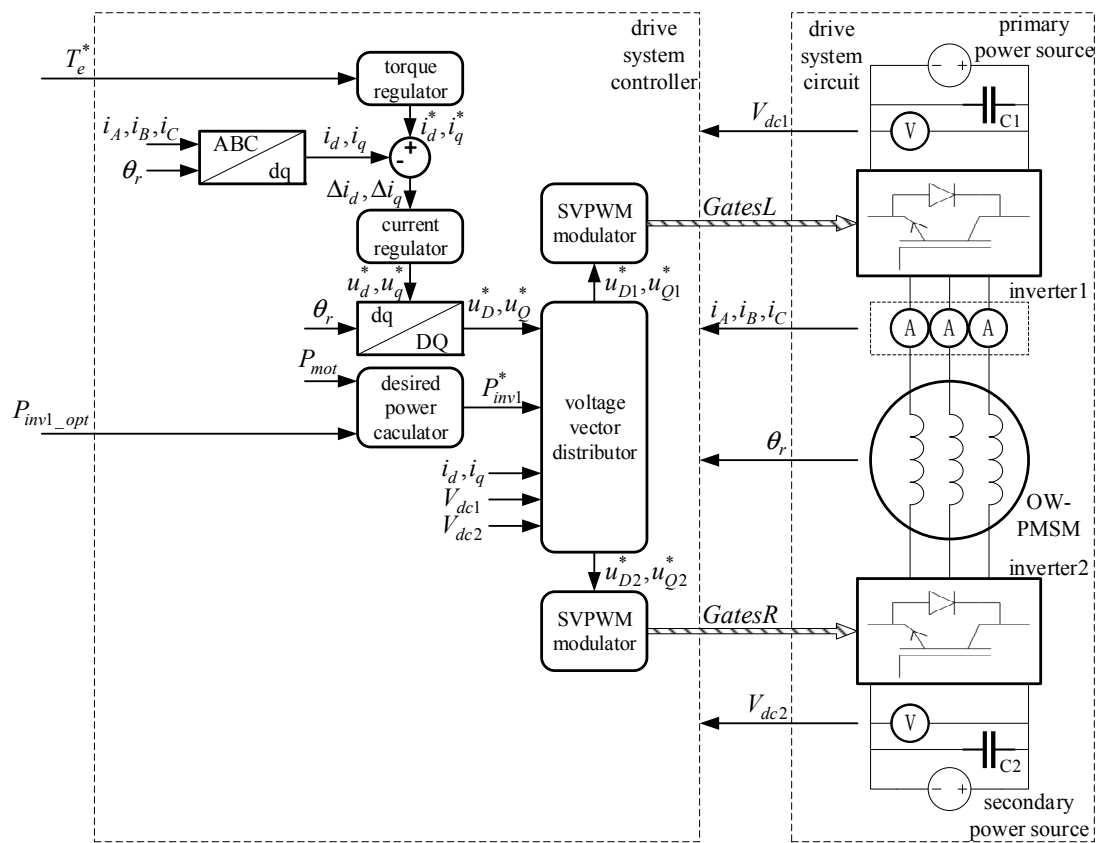


Figure 10. Overall configuration of the proposed system.

In the drive system controller, the desired torque  $T_e^*$  and the optimal output power of inverter1  $P_{inv1\_opt}$  are inputted from vehicle control unit. In torque regulator, the desired stator current  $i_s^*$  is calculated by MTPA (maximum torque per ampere) method in constant torque region and CBE (constant back EMF) method in flux weakening region [26,27]. Then the desired stator voltage vector  $u_s^*$  is generated by the current regulator, which is actual a PI controller. The desired power sharing calculation method introduced in sector 3 is executed in the desired power calculator, outputting desired output power of inverter1  $P_{inv1}^*$ . Afterwards, the voltage vector distribution method expounded in sector 4 is carried out in the voltage vector distributor. After the desired stator voltage vector is partitioned, the desired voltage vectors of inverter1 and inverter2, known as  $u_{s1}^*$  and  $u_{s2}^*$ , are sent to the corresponding SVPWM modulators respectively. Where  $GatesL$  and  $GatesR$  are the gate control signals for inverter1 and inverter2 respectively.

### 5.2. Simulation Results

To validate to proposed control methods, we ran a simulation of the OW-PMSM drive system on Matlab/Simulink platform. The basic parameters of the drive system circuit are shown in Table 2 and the controller parameters are shown in Table 3. It is important to note that an extra motor speed controller, which is actual a PI controller, was used to generate the desired torque  $T_e^*$  inputted to the torque regulator mentioned above to make the motor speed follow the preset value. This motor speed controller is not necessary in an electric vehicle and not shown in Figure 10.

**Table 2.** Parameters of the drive system circuit. OW-PMSM: open-end winding permanent magnet synchronous motor.

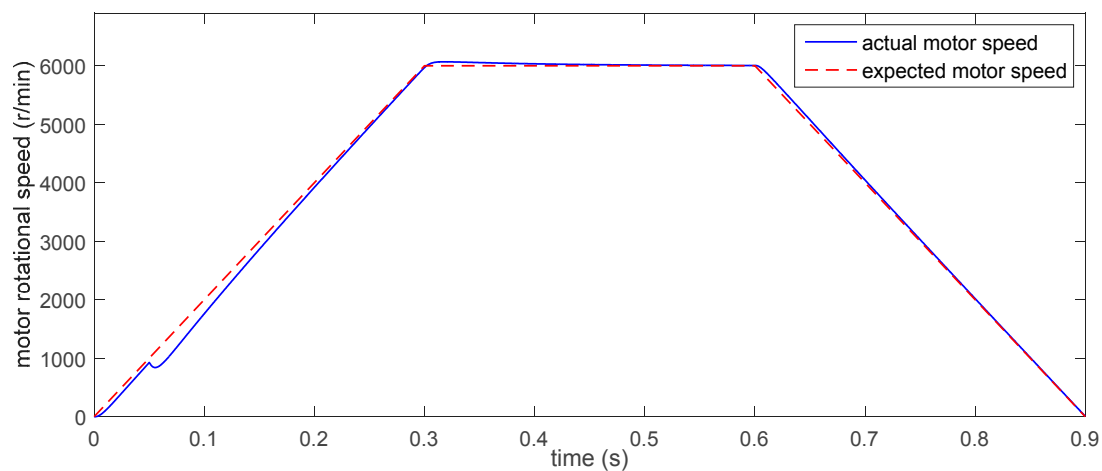
Modules	Items	Parameters
Solver	Solve type	Discrete
	Time step $T_s/s$	$5 \times 10^{-7}$
OW-PMSM	Motor type	Interior open-end winding PMSM
	Number of pole pairs $p_0$	4
	Stator resistance $R_s/\Omega$	0.1
	Fundamental amplitude and third harmonic amplitude of permanent magnet flux linkage $[\psi_f, \psi_{f3}]/Wb$	[0.2, 0.01]
	d-axis and q-axis inductance $[L_d, L_q]/F$	[0.0012, 0.0015]
	Zero sequence inductance $L_0/F$	0.0003
	Rotational inertia of rotor $J_m/kg\ m^{-2}$	0.011
	Cullen and viscous resistance coefficient	[0.001, 0.0005]
Inverter devices	On-resistance $R_{on}/\Omega$	0.01
	Forward voltage drop $V_f/V$	0.8
	Current fall time and tailing time $[T_f, T_t]/s$	$[1, 1.5] \times 10^{-6}$
	Current capacity of each phase $i_{max}/A$	160
Power Sources	DC-bus voltages of primary and secondary power source $[V_{dc1}, V_{dc2}]/V$	[300, 200]

**Table 3.** Parameters of the drive system controller. SVPWM: space vector pulse width modulation.

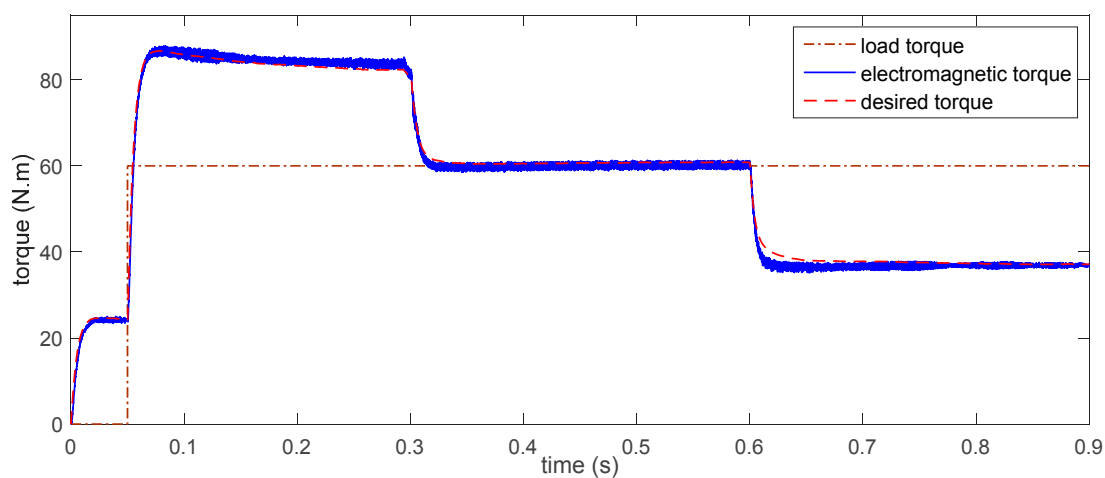
Modules	Items	Parameters
Motor speed controller	Sampling time $T_{s\_SC}/s$	$1 \times 10^{-4}$
	Proportionality coefficient $P_{SC}$	0.2
	Integral coefficient $I_{SC}$	2
Torque regulator	Sampling time $T_{s\_TR}/s$	$1 \times 10^{-4}$
	Voltage saturation coefficient $k_u$	0.95
Current regulator	Sampling time $T_{s\_CR}/s$	$1 \times 10^{-4}$
	Proportionality coefficient $P_{CR}$	2
	Integral coefficient $I_{CR}$	120
Desired power calculator	Sampling time $T_{s\_PC}/s$	$1 \times 10^{-4}$
	Gain of the inertial element $K_{PC}$	0.5
	Time constant of the inertial element $T_{PC}/s$	0.05
Voltage vector distributor	Sampling time $T_{s\_VD}/s$	$1 \times 10^{-4}$
	Maximum power difference of inverter1 $D_{Pinv1\_max}/kW$	3
SVPWM modulator	Sampling time $T_{s\_SVM}/s$	$1 \times 10^{-4}$
	Control period $T_{c\_SVM}/s$	$1 \times 10^{-4}$

This simulation’s duration was 0.9 s. The expected motor speed linearly increased from 0 to 6000 r/min in 0–0.3 s and stayed at 6000 r/min till 0.6 s. Then the speed linearly dropped to 0 in 0.6–0.9 s. The load torque jumped from 0 to 60 N·m at 0.05 s and remained until simulation finished.

Curves of motor’s expected and actual rotational speed are shown in Figure 11a, curves of motor’s desired torque, electromagnetic torque, and load torque are shown in Figure 11b.



(a) Expected and actual rotational speed of motor.



(b) Desired torque, electromagnetic torque, and load torque of motor.

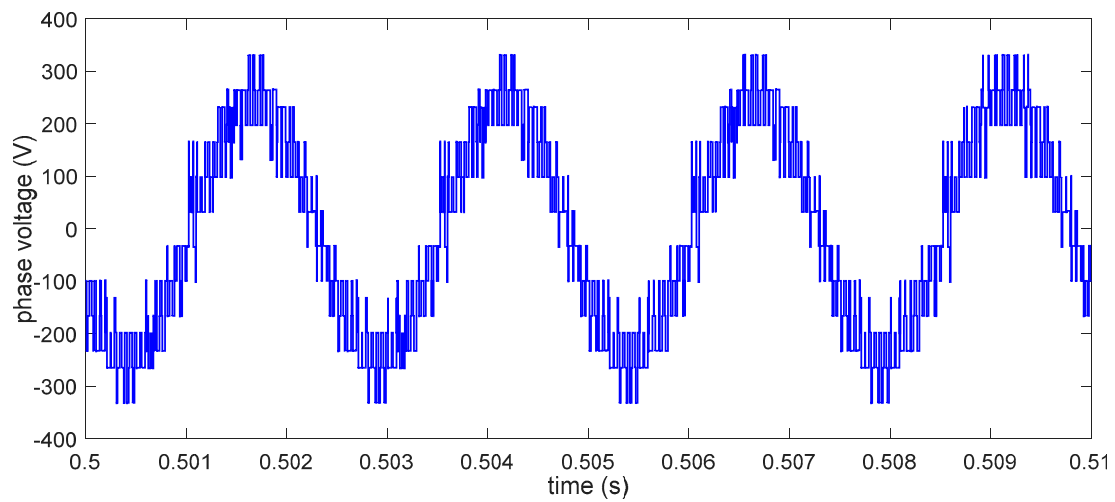
**Figure 11.** Curves of motor speed and torque.

We can observe from Figure 11a that the motor rotary speed could smoothly and swiftly follow the preset value and only had a slight fluctuation at 0.05 s when the load torque jumped. Figure 11b also indicates that motor's electromagnetic torque followed the desired torque well, the amplitude its fluctuation was limited within 3 N·m under dual inverter's modulation by SVPWM strategy with an operating frequency of 10 kHz. The torque's fluctuation was reduced by about 50% compared to the multi-level current hysteresis modulation we proposed in [24].

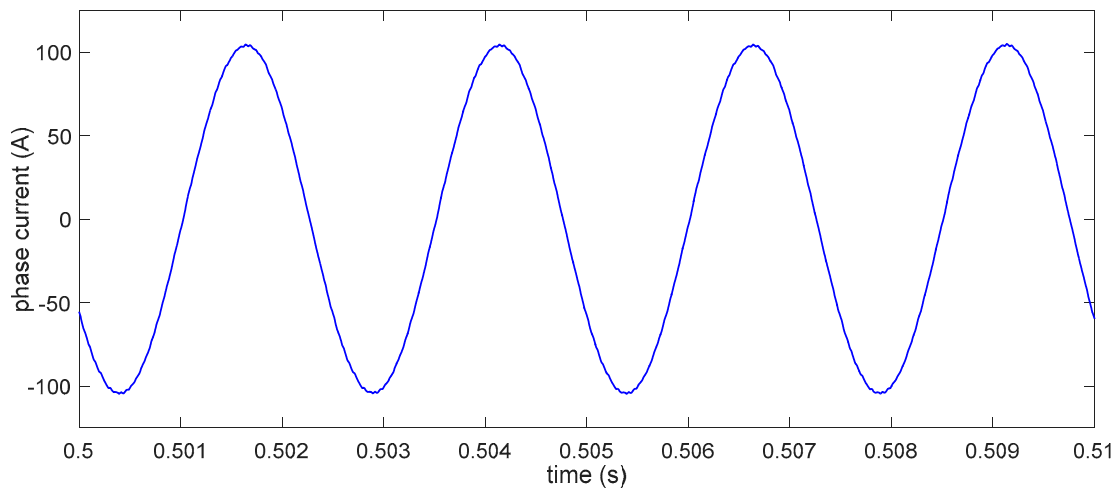
Local curves of phase A's voltage and current are shown in Figure 12a,b respectively, with a time range of 0.5–0.51 s.

Theoretically, there are five levels in motor's phase voltage of a single inverter system under SVPWM strategy. In a dual inverter system, if the two DC-bus voltages are equal, there are nine levels in motor's phase voltage. Furthermore, there are even more phase voltage levels with unequal DC-bus voltages. These additional levels made the waveform of phase A's voltage shown in Figure 12a more close to the sine wave, compared to a single inverter system. Figure 12b also shows the current ripple was reduced significantly, compared to the system under the multi-level current hysteresis modulation [24].

In addition, we made a harmonic analysis of phase A's voltage in the time range of 0.35–0.55 s, while the motor was working in a steady state at the speed of 6000 r/min. The result is shown in Figure 13.



(a) Phase A's voltage in 0.5–0.51 s.



(b) Phase A's current in 0.5–0.51 s.

**Figure 12.** Local curves of phase A's voltage and current and harmonic component.

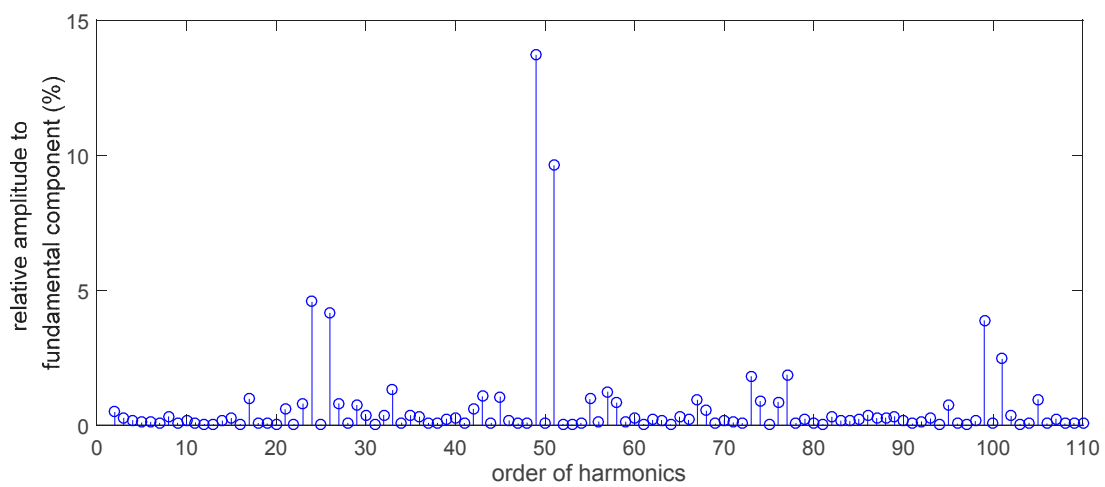
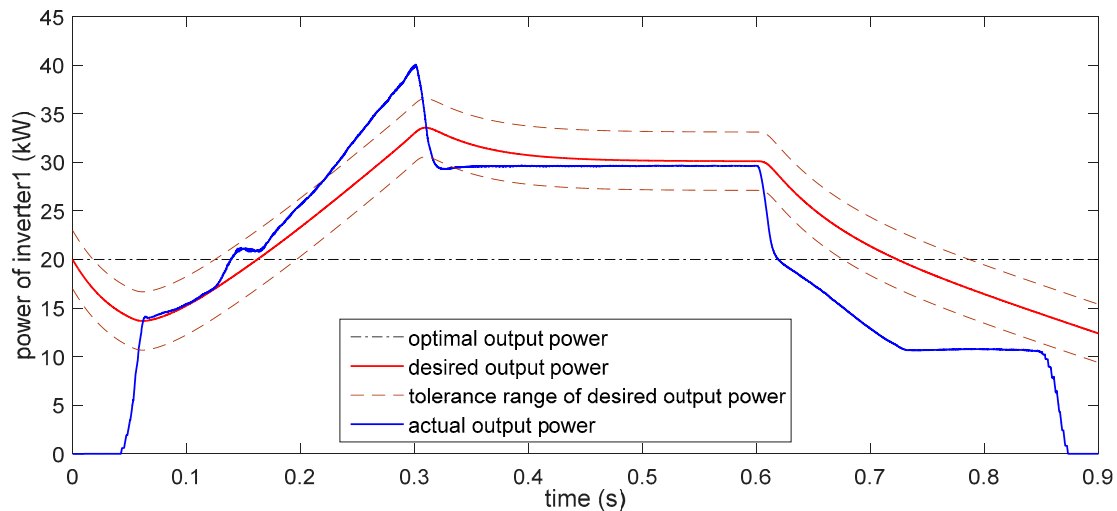


**Figure 13.** Relative amplitude to fundamental component of phase A's voltage in 0.35–0.55 s.

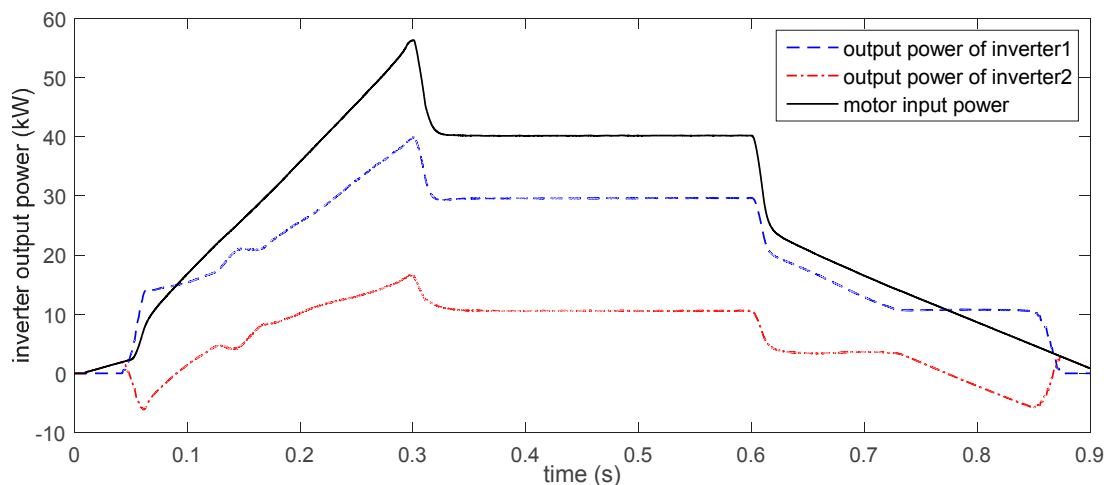
From Figure 13 we can see, the proportion of the harmonic components are very low and mainly concentrate around 25th harmonic and its multiples. The components around 50th harmonic

are relatively large, with amplitudes above 10% of the fundamental amplitude. Considering the fundamental frequency is 400 Hz (rotor rotate speed multiplies number of pole-pairs), the frequency of the 50th harmonic is 20 kHz, which is just twice as the SVPWM control frequency.

Curves in regard to inverter1’s output power following effect, and curves of two inverters’ output power are shown in Figure 14a,b respectively.



(a) Optimal, desired, and actual output power of inverter1.



(b) Output power of two inverters.

Figure 14. Curves of inverter output power.

From Figure 14a we can see, while inverter1’s optimal output power  $P_{inv1\_opt}$  was fixed at 20 kW as a constant, the desired output power  $P_{inv1}^*$  had some fluctuations to approach the motor input power shown in Figure 13b, which relieved the power outputting stress on inverter2. Due to the inertial element in the desired power calculator, the curve of  $P_{inv1}^*$  never went too far from  $P_{inv1\_opt}$  and had a moderate fluctuation, which had a positive effect on the primary power source’s efficiency performance. The tolerance range of inverter1’s power following, which is determined by  $[P_{inv1}^* - D_{P_{inv1\_max}}, P_{inv1}^* + D_{P_{inv1\_max}}]$ , is indicated by the dashed lines. Within this range, inverter1’s output power was considered following  $P_{inv1}^*$  accurately enough, thus the low switching frequency method was selected in priority to reduce inverter1’s switching frequency. Most of the time, inverter1’s actual output power stayed in the tolerance range as expected. However, in first 0.05 s and after the motor speed started going down, inverter1’s actual output power couldn’t follow  $P_{inv1}^*$  well. Because during these periods, motor’s load torque was too low to demand a stator current vector with an

enough amplitude for the power distribution in a big ratio or power transfer between the two power sources. The stator current is the medium of power transfer through the motor, thus a stator current vector with a considerable amplitude is necessary for the power distribution in a wide range or power transfer between the two power sources. In other words, the range of power distribution ratio or power transfer between the two power sources is limited by the amplitude of motor’s stator current vector, which is also determined by motor’s load torque. This limitation was discussed in [23], but it’s not completely suitable for the circumstance here.

As shown in Figure 14b, the motor’s input power was determined by motor’s speed demand and the load torque, and was the summation of the two inverters’ output power. While inverter1’s output power was controlled to follow  $P_{inv1}^*$ , inverter2’s output power was made to compensate the lacking power or absorb the redundant power. During some periods where inverter1’s output power was more than motor’s requirement, inverter2’s output power was negative, meaning inverter2 was absorbing power. In other words, the primary power source was charging the secondary power source through the motor.

We define the voltage vector distribution mode number to specify the status of voltage vector distribution. Relations between the mode number and the specific circumstances of voltage vector distribution are listed in Table 4. And the curve of voltage vector distribution mode number is shown in Figure 15.

Table 4. Meanings of voltage vector distribution mode number.

Voltage Vector Distribution Method	Specific Circumstance	Mode Number
Low switching frequency method	The nth candidate vector is selected (the mode number indicates the ranking of selected vector in the sorted sequence)	1~7
Accurate power following method	inverter1’s power following deviation $D_{P_{inv1\_AF}}$ equals to 0	0
	inverter1’s power following deviation $D_{P_{inv1\_AF}}$ is not equal to 0	-1
Linear partition method	inverter1’s power following deviation $D_{P_{inv1\_LP}}$ equals to 0	-2
	inverter1’s power following deviation $D_{P_{inv1\_LP}}$ is not equal to 0, but $\vec{u}_s^*$ can be integrally synthesized	-3
	$\vec{u}_s^*$ cannot be integrally synthesized	-4

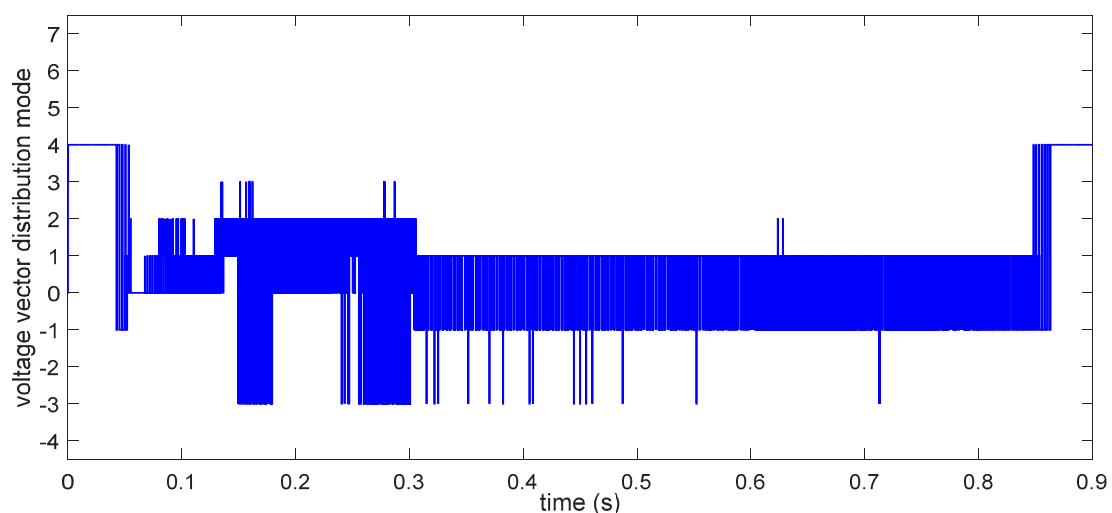


Figure 15. Curve of voltage vector distribution mode number.

As shown in Figure 15, some values of the mode number never appeared, such as  $-4, 5, 6,$  and  $7$ . The absence of  $-4$  is because in this simulation, the amplitude of  $\vec{u}_s^*$  was not too high and the DC-bus voltages of the two power sources were enough, thus  $\vec{u}_s^*$  could always be integrally synthesized. In low switching frequency method, inverter1's output power values corresponding to the candidate voltage vectors ranked behind were not in the tolerance range of inverter1's power following. Thus the absence of  $5, 6, 7$  is mostly decided by this tolerance range. The narrower this range is, the fewer the candidate voltage vectors can be selected.

The voltage vector distribution of inverter1 and inverter2 in static DQ plane are shown in Figure 16a,b respectively, with a sampling step of  $0.002$  s. The curves of inverter switching frequency and inverter losses are shown in Figure 17a,b respectively.

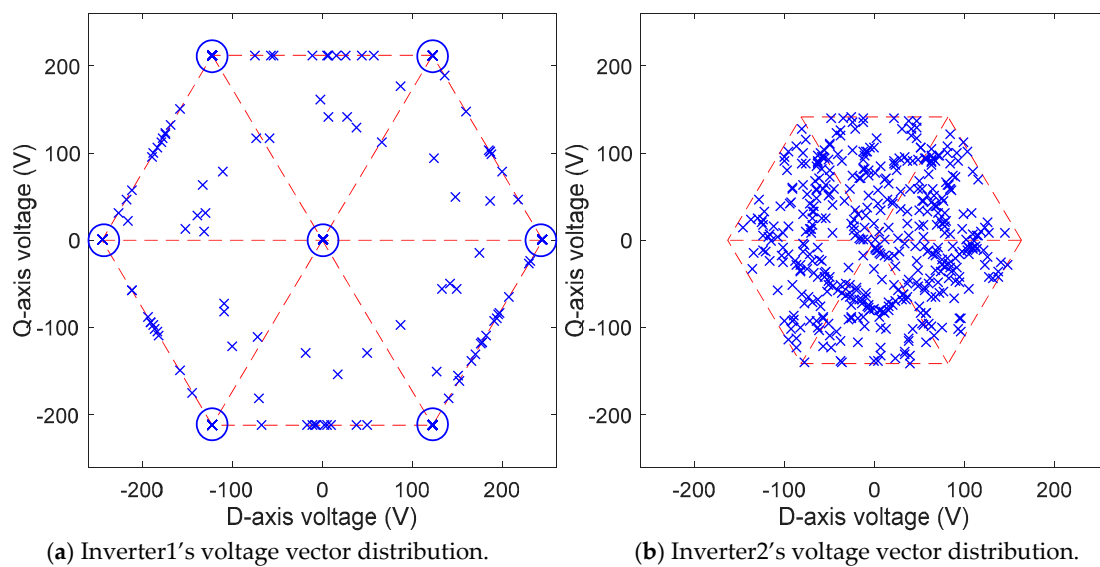
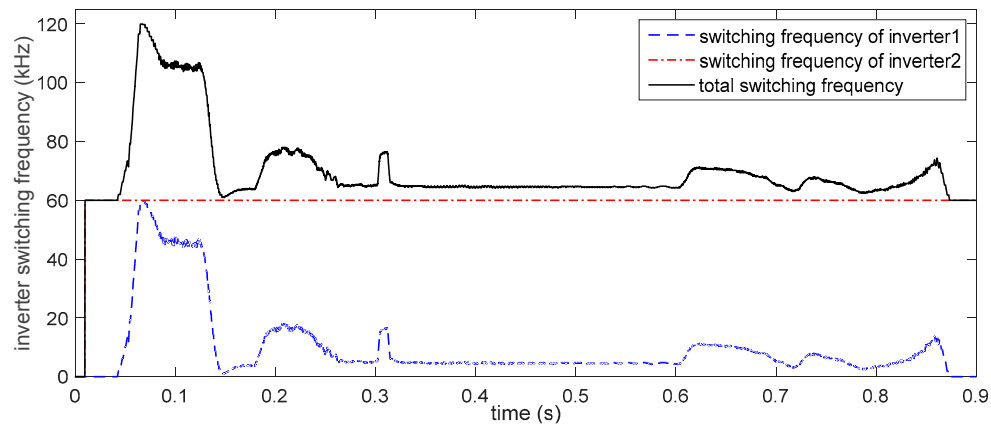


Figure 16. Inverter voltage vector distribution in static DQ plane.

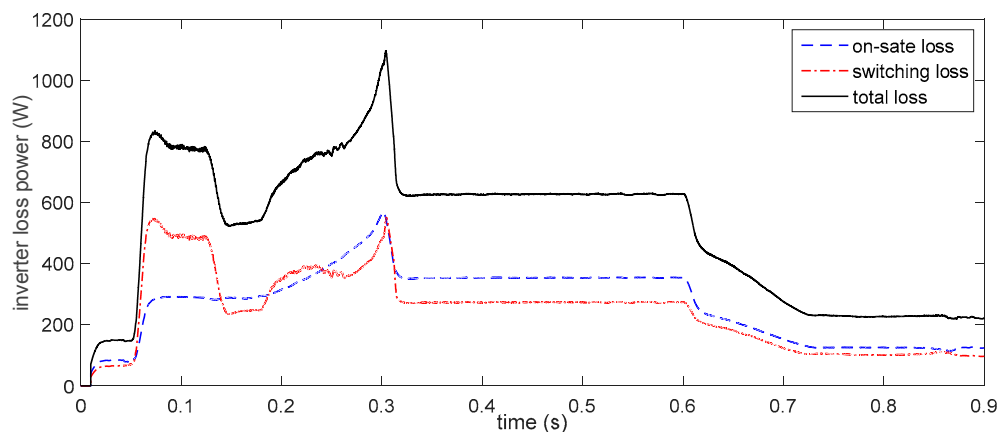
From Figure 16 we can see, all the sampled voltage vectors, noted as “x”, were within the modulation range of the corresponding inverter, indicated by the dashed hexagon, as expected. However, the distribution characteristics of these voltage vectors are different between inverter1 and inverter2. In Figure 16a, many sampled voltage vectors overlapped at the circled positions, which are the vertexes and the center of inverter1's hexagon, where the candidate voltage vectors of low switching frequency method are lying. That is because during most of the simulation time, the low switching frequency method was selected, which can be discovered from Figure 15. For this reason, the sampled voltage vectors of inverter1 appeared sparser than inverter2's shown in Figure 16b, while their amount were actually the same. We can also discover that there was a certain amount of sampled voltage vectors on the boundary of inverter1's modulation range. That is because sometimes inverter1's output power was hard to stay in its tolerance range, on these occasions inverter1 had to generate the voltage vector with highest amplitude to make its output power closer to the tolerance range. Relatively, as Figure 16b shows, the sampled voltage vectors of inverter2 were almost uniformly distributed due to inverter2's role of a compensator.

In a large proportion of the simulation time inverter1 was outputting basic voltage vectors and saturated voltage vectors, of which the switch commutations in a SVPWM period are fewer than regular voltage vectors. This resulted in the switching frequency of inverter1 much lower than inverter2, especially in the steady state operation when motor's speed and electromagnetic torque were not changing, as shown in Figure 17a. The inverter losses consist of the on-state loss and the switching loss, in which the on-state loss is only determined by the current through the inverter, while the switching loss is in direct proportion to the inverter switching frequency. From Figure 17b we can see most of the

time the switching loss was lower than the on-state loss due to inverter1's low switching frequency, resulting in the improvement of inverter efficiency.



(a) Total switching frequency of inverter devices.



(b) On-state loss and switching loss power of inverter.

Figure 17. Curves of inverter switching frequency and inverter loss power.

## 6. Conclusions

This paper, aims at an OW-PMSM drive system fed by dual inverter for electric vehicles, in which each inverter is powered by an independent power source. The primary power source is an energy conversion device while the secondary power source consists of an energy storage element. A desired power sharing calculation method has been proposed. By using a first order inertial element, it could manage the power sharing between the two power sources to optimize the energy efficiency of the primary power source. Furthermore, three different voltage vector distribution methods with various advantages have been proposed, and their selection strategy could select the optimal one according to the operating conditions. Based on the integral synthesizing of the desired stator voltage vector, the proposed voltage vector distribution method could reduce the inverter switching frequency while making the primary power source follow its desired output power. Finally, a simulation of the drive system on Matlab/Simulink platform has been executed to validate the proposed methods.

The proposed system is suitable for electric vehicles with a single motor driving and powered by two power sources, so that the power flow can be handled by the dual inverter and OW-PMSM without a DC/DC converter and the DC voltage is lowered. The desired power sharing calculation method and voltage vector distribution method could improve the primary power source's energy efficiency by regulating its output power and lessen inverter1's switching loss by reducing its switching frequency,

respectively. By controlling the optimal output power of inverter1 inputted to the system, they could also handle the energy management between the two power sources. The proposed methods provide a theoretical basis and implementation scheme for a dual inverter OW-PMSM drive system with two isolated power sources in electric vehicles.

Future research will be directed towards finding an energy management method matched with this system for electric vehicles to maximize the overall efficiency and driving range, and extending the ranges of power sharing or power transfer between two power sources when the load torque is not high enough. After solving the existing practical issues, an experimental verification of the proposed system will also be executed in an electric vehicle.

**Acknowledgments:** This work was supported by the China Postdoctoral Science Foundation (2014M561290), the Energy Administration of Jilin Province [2016]35, the Jilin Province Science and Technology Development Fund (20150520115JH), the Jilin Province Science and Technology Development Fund (20180101062JC), and Energy Conservation and Ecological Protection of Special Funds Project of Jilin Province (2017).

**Author Contributions:** Nan Xu and Yi-Fan Jia conceived the control method and wrote the full manuscript; Yu-Kuan Li and Di Zhao performed the simulation and revised the manuscript; Xin Tang analyzed the data; Liang Chu analyzed and evaluated the simulation results and gave valuable suggestions.

**Conflicts of Interest:** The authors declare no conflict of interest.

## References

1. Park, J.W.; Koo, D.H.; Kim, J.M.; Kim, H.G. Improvement of control characteristics of interior permanent magnet synchronous motor for electric vehicle. *IEEE Trans. Ind. Appl.* **2001**, *37*, 1754–1760. [[CrossRef](#)]
2. Boazzo, B.; Pellegrino, G. Model-based direct flux vector control of permanent-magnet synchronous motor drives. *IEEE Trans. Ind. Appl.* **2015**, *51*, 3126–3136. [[CrossRef](#)]
3. Park, C.S.; Lee, J.S. A torque error compensation algorithm for surface mounted permanent magnet synchronous machines with respect to magnet temperature variations. *Energies* **2017**, *10*, 1365. [[CrossRef](#)]
4. Nam, K.-T.; Kim, H.; Lee, S.-J.; Kuc, T.-Y. Observer-Based Rejection of Cogging Torque Disturbance for Permanent Magnet Motors. *Appl. Sci.* **2017**, *7*, 867. [[CrossRef](#)]
5. Wu, H.X.; Li, L.Y.; Kou, B.Q.; Ping, Z. The research on energy regeneration of permanent magnet synchronous motor used for hybrid electric vehicle. In Proceedings of the Vehicle Power and Propulsion Conference (VPPC '08), Harbin, China, 3–5 September 2008; pp. 1–4. [[CrossRef](#)]
6. Howlader, A.M.; Urasaki, N.; Senjyu, T.; Yona, A.; Saber, A.Y. Optimal pam control for a buck boost dc-dc converter with a wide-speed-range of operation for a PMSM. *J. Power Electron.* **2010**, *10*, 477–484. [[CrossRef](#)]
7. Athavale, A.; Sasaki, K.; Gagas, B.S.; Kato, T.; Lorenz, R. Variable flux permanent magnet synchronous machine (VF-PMSM) design methodologies to meet electric vehicle traction requirements with reduced losses. *IEEE Trans. Ind. Appl.* **2017**, 1–8. [[CrossRef](#)]
8. Howlader, A.M.; Urasaki, N.; Senjyu, T.; Yona, A. Wide-Speed-Range optimal PAM control for permanent magnet synchronous motor. In Proceedings of the IEEE International Conference on Electrical Machines and Systems, Tokyo, Japan, 15–18 November 2009; Volume 2007, pp. 1–5.
9. Li, Z.; Onar, O.; Khaligh, A.; Schartz, E. Design and control of a multiple input DC/DC converter for battery/ultra-capacitor based electric vehicle power system. In Proceedings of the IEEE Applied Power Electronics Conference and Exposition, Washington, DC, USA, 15–19 February 2009; pp. 591–596.
10. Gualous, H.; Gustin, F.; Berthon, A.; Dakyo, B. DC/DC converter design for supercapacitor and battery power management in hybrid vehicle applications—Polynomial control strategy. *IRE Trans. Ind. Electron.* **2010**, *57*, 587–597. [[CrossRef](#)]
11. An, Q.; Liu, J.; Peng, Z.; Sun, L.; Sun, L. Dual-space vector control of open-end winding permanent magnet synchronous motor drive fed by dual inverter. *IEEE Trans. Power Electron.* **2016**, *31*, 8329–8342. [[CrossRef](#)]
12. Nguyen, N.K.; Semail, E.; Meinguet, F.; Sandulescu, P.; Kestelyn, X.; Aslan, B. Different virtual stator winding configurations of open-end winding five-phase PM machines for wide speed range without flux weakening operation. In Proceedings of the IEEE European Conference on Power Electronics and Applications, Lille, France, 2–6 September 2013; pp. 1–8.
13. Sandulescu, P.; Meinguet, F.; Kestelyn, X.; Semail, E.; Bruyere, A. Control strategies for open-end winding drives operating in the flux-weakening region. *IEEE Trans. Power Electron.* **2014**, *29*, 4829–4842. [[CrossRef](#)]

14. Kwak, M.S.; Sul, S.K. Flux weakening control of an open winding machine with isolated dual inverters. In Proceedings of the IEEE Industry Applications Conference 2007, New Orleans, LA, USA, 23–27 September 2007; pp. 251–255.
15. Welchko, B.A. A double-ended inverter system for the combined propulsion and energy management functions in hybrid vehicles with energy storage. In Proceedings of the IEEE Industrial Electronics Society, Raleigh, NC, USA, 6–10 November 2005; p. 6.
16. Machiya, H.; Haga, H.; Kondo, S. High efficiency drive method of an open-winding induction machine driven by dual inverter using capacitor across dc bus. *Electr. Eng. Jpn.* **2016**, *197*, 62–72. [[CrossRef](#)]
17. Drisya, V.; Samina, T. Supply voltage boosting using a floating capacitor bridge in a 3 level space vector modulated inverter system for an open-end winding induction motor drive. In Proceedings of the IEEE International Conference on Control Communication & Computing, Trivandrum, India, 19–21 November 2015; pp. 165–169.
18. Sivakumar, K.; Das, A.; Ramchand, R.; Patel, C.; Gopakumar, K. A hybrid multilevel inverter topology for an open-end winding induction-motor drive using two-level inverters in series with a capacitor-fed h-bridge cell. *IRE Trans. Ind. Electron.* **2010**, *57*, 3707–3714. [[CrossRef](#)]
19. Pan, D.; Huh, K.K.; Lipo, T.A. Efficiency improvement and evaluation of floating capacitor open-winding PM motor drive for EV application. In Proceedings of the IEEE Energy Conversion Congress and Exposition, Pittsburgh, PA, USA, 14–18 September 2014; pp. 837–844.
20. Park, J.S.; Nam, K. Dual Inverter Strategy for High Speed Operation of HEV Permanent Magnet Synchronous Motor. In Proceedings of the IEEE Industry Applications Conference, Tampa, FL, USA, 8–12 October 2006; Volume 1, pp. 488–494.
21. Sun, D.; Zheng, Z.; Lin, B.; Zhou, W.; Chen, M. A hybrid PWM based field weakening strategy for hybrid-inverter driven open-winding PMSM system. *IEEE Trans. Power Appar. Syst.* **2017**, 2912–2918. [[CrossRef](#)]
22. Griva, G.; Oleschuk, V. Flexible PWM control of three-level inverters for fuel cell/battery supplied aeromobile drive. In Proceedings of the IEEE Industrial Electronics, Porto, Portugal, 3–5 November 2009; pp. 3735–3740.
23. Casadei, D.; Grandi, G.; Lega, A.; Rossi, C. Multilevel operation and input power balancing for a dual two-level inverter with insulated DC sources. *IEEE Trans. Ind. Appl.* **2008**, *44*, 1815–1824. [[CrossRef](#)]
24. Chu, L.; Jia, Y.F.; Chen, D.-S.; Xu, N.; Wang, Y.-W.; Tang, X.; Xu, Z. Research on Control Strategies of an Open-End Winding Permanent Magnet Synchronous Driving Motor (OW-PMSM)-Equipped Dual Inverter with a Switchable Winding Mode for Electric Vehicles. *Energies* **2017**, *10*, 616. [[CrossRef](#)]
25. Hendawi, E.; Khater, F.; Shaltout, A. Analysis, simulation and implementation of space vector pulse width modulation inverter. In Proceedings of the WSEAS International Conference on Applications of Electrical Engineering, World Scientific and Engineering Academy and Society (WSEAS), Penang, Malaysia, 23–25 March 2010; pp. 124–131.
26. Sun, T.; Wang, J.; Chen, X. Maximum torque per ampere (MTPA) control for interior permanent magnet synchronous machine drives based on virtual signal injection. *IEEE Trans. Power Electron.* **2015**, *30*, 5036–5045. [[CrossRef](#)]
27. Hu, D.; Zhu, L.; Xu, L. Maximum Torque per Volt operation and stability improvement of PMSM in deep flux-weakening Region. In Proceedings of the IEEE Energy Conversion Congress and Exposition, Raleigh, NC, USA, 15–20 September 2012; pp. 1233–1237.

